FACULTY
OF MATHEMATICS
AND PHYSICS
Charles University

MASTER THESIS

Jozef Lipták

Spectroscopic study of eccentric eclipsing binaries

The Astronomical Institute of Charles University

Supervisor of the master thesis: doc. RNDr. Marek Wolf, CSc.

Study programme: Astronomy and Astrophysics
(N0533A110009)

Study branch: Astronomy and Astrophysics
(FAAP)

Prague 2022

I declare that I carried out this master thesis independently, and only with the cited sources, literature and other professional sources. It has not been used to obtain another or the same degree.

I understand that my work relates to the rights and obligations under the Act No. 121/2000 Sb., the Copyright Act, as amended, in particular the fact that the Charles University has the right to conclude a license agreement on the use of this work as a school work pursuant to Section 60 subsection 1 of the Copyright Act.

In . . . . date . . . .
                                                                                   Author's signature

Title: Spectroscopic study of eccentric eclipsing binaries

Author: Jozef Lipták

Institute: The Astronomical Institute of Charles University

Supervisor: doc. RNDr. Marek Wolf, CSc., The Astronomical Institute of Charles University

Abstract: Close eccentric eclipsing binary star systems are important to our understanding of stellar formation and evolution. We analyze three such systems - V335 Ser, BW Boo and DR Vul - with emphasis on a possible third body in the systems needed for the system's existence according to the current theoretical models. Using spectra from the Ondřejov Observatory, we attempted to disentangle the spectra of the components and determine the radial velocity solutions for the systems. For V335 Ser we obtain new radial velocity measurements, spectra, and upper limits on the mass of a possible third body. For BW Boo we obtain the spectrum of the third body possibly dynamically connected with the system. Using measured radial velocities and our fit to TESS photometry, we compute best to date parameters for the components and the orbit of the binary system. In the system DR Vul we confirmed the third body and also its nature by obtaining its spectra. We present the first orbital solution available for the central binary. The triple system does not seem to follow the theoretically predicted common inclination of the orbits.

Keywords: spectroscopy, photometry, eclipsing binary stars, multiple star systems, stellar statistics

Contents

Introduction

Origin and evolution of multiple star systems is a hot topic in astrophysics. Current hydrodynamical and N-body simulations did not explain the population of short period eccentric binaries. Orbits of such systems should be circularised by the friction in common envelope/disk during the fase of accretion. Moreover sometimes we observe stars that are closer toghether than the physical size of them in protostar stage would allow. Most prevalent explanation of existence of these systems is orbital evolution of the system after the formation by Kozai-Lidov cycles with tidal friction. Therefore it is expected to find the third body driving the Kozai mechanism in the eccentric systems with period of order of days.

  We are going to focus on three short period eclipsing binary systems V335 Ser, BW Boo and DR Vul where at least one component is of an early spectral type. These systems have red linear spectra in the Ondřejov Observatory archive avaiable which were not yet analysed. Using `KOREL` software we aim to disentangle the spectra of the binaries and look for the possible spectra of third bodies in the systems. In case of DR Vul where the third body was already detected using eclipse timing variation method our goal is to confirm the companion and indetify it's nature. Next we aim to obtain orbital elements and physical characteristics of the component stars. To do so we are using published photometric studies of the systems and in case of BW Boo we are attempting our own model of TESS lightcurve done using software `PHOEBE`.

  The tesis is divided into three parts, first (1) contains mainly theoretical description of multiple star system dynamic, formation and evolution needed for our work toghether with some additional useful concepts. Second part (2) describes software and methodology used in our work concentrating on practical description of steps taken. Final part (3) contains summaries of published articles, details on data used and results of our work consecutively for the three systems.

1. Theoretical introduction

1.1 Double stars as point masses

Binary star systems can, as the first approximation, be modeled as point mass systems under the Isaac Newton's theory of gravity. This approximation is valid with increasing separation between stars with a great advantage of Isaac Newton's shell theorem for spherically symmetric sources and high density concentration of stellar mass towards their centers. The solution of equations of motion is a well-known solution to the Kepler problem: in the case of a bounded system, the bodies orbit around their common center of mass on planar generally elliptical orbits with fixed orientation in space. Commonly we describe the position of a secondary body with respect to the primary body, which is usually more massive. If we place the primary body in the origin of the coordinate frame, the shape of the orbit is given by the polar equation of the conic section for polar coordinates $\mathbf{r} = (r, \nu)$

$$r = \frac{a(1 - e^2)}{1 + e \cos \nu} \,, \tag{1.1}$$

where a is the semimajor axis of the relative orbit and e is its numerical eccentricity. Angular coordinate ν is called the true anomaly.

Denoting the gravitational constant as G, mass of primary as M_1, mass of secondary as M_2, and orbital period P we have Kepler's third law

$$\frac{a^3}{P^2} = \frac{G(M_1 + M_2)}{4\pi^2} \,. \tag{1.2}$$

The temporal evolution of the system is given by series of following equations for mean anomaly M, eccentric anomaly E and true anomaly ν

$$M(t) = 2\pi \frac{t - T_0}{P} \,, \tag{1.3}$$

$$E(t) = M(t) + e \sin E(t) \,, \tag{1.4}$$

$$\tan \frac{\nu(t)}{2} = \sqrt{\frac{1 + e}{1 - e}} \tan \frac{E(t)}{2} \,, \tag{1.5}$$

where T_0 is the point of zero time called epoch. We measure M, E, ν in radians. It's important to point out that so called Kepler's equation 1.4 for eccentric anomaly must be solved numerically. Distance between bodies is then given by equation 1.1.

For motion in space, we need to consider a few additional facts:

- center of mass of the system is moving uniformly in a straight line

- vector $\mathbf{r}$ connecting the bodies is divided by the center of mass in the inverse ratio of masses of the bodies

$$\mathbf{r_1} M_1 = -\mathbf{r_2} M_2 \,, \qquad \mathbf{r} = \mathbf{r_2} - \mathbf{r_1} \,, \tag{1.6}$$

where $\mathbf{r_1}$, $\mathbf{r_2}$ are radius vectors of the bodies relative to the center of mass.

1.1.1 Radial velocities

Using spectroscopic measuremets, we can use the Doppler shift formula

$$\frac{\Delta\lambda}{\lambda} = \frac{v}{c} \tag{1.7}$$

to obtain velocities of the bodies v along the line of sight - radial velocities. From the equation of orbit 1.1, equations 1.3 to 1.5 for temporal evolution and facts closing previous chapter, we get the radial velocity of primary and secondary as

$$RV_1 = \gamma + K_1(\cos(\nu(t) + \omega_1) + e\cos\omega_1)\,, \tag{1.8}$$
$$RV_2 = \gamma - K_2(\cos(\nu(t) + \omega_2) + e\cos\omega_2)\,, \tag{1.9}$$

where $\omega_2 = \omega_1 + \pi$ are longitudes of periastron, K_1, K_2 are semiaplitudes of radial velocity and γ is radial velocity of the center of mass relative to the observer. Parameters K_1, K_2, ω_1, ω_2, e, T_0, P and γ can be directly fitted from observed radial velocity curves.

For the semiamplitudes we obtain the following relations

$$a_1 \sin i = \frac{P}{2\pi} K_1 \sqrt{1 - e^2}\,, \tag{1.10}$$

$$a_2 \sin i = \frac{P}{2\pi} K_2 \sqrt{1 - e^2}\,, \tag{1.11}$$

where i is the inclination of the orbital plane of binary and a_1, a_2 are the semimajor axis of respective orbits connected to the semimajor axis of the relative orbit a by

$$a_1 = a \frac{M_2}{M_1 + M_2}\,, \tag{1.12}$$

$$a_2 = a \frac{M_1}{M_1 + M_2}\,. \tag{1.13}$$

We can add equations 1.10 together and using equation 1.2 obtain the masses of the components

$$M_1 \sin^3 i = \frac{K_2(K_1 + K_2)^2 P\left(1 - e^2\right)^{\frac{3}{2}}}{2\pi G}\,, \tag{1.14}$$

$$M_2 \sin^3 i = \frac{K_1(K_1 + K_2)^2 P\left(1 - e^2\right)^{\frac{3}{2}}}{2\pi G}\,. \tag{1.15}$$

We can see that masses can not be determined exactly if we do not know the inclination of the system. We cannot obtain inclination from spectroscopic observation alone; it must be obtained from astrometry in the case of visual binaries or photometry in the case of eclipsing binaries, or by some other method.

If we observe spectral lines of only one component (usually brighter more masive primary) we can determine only so-called mass function $f(M)$

$$f_1(M) = \frac{K_1^3 P\left(1 - e^2\right)^{\frac{3}{2}}}{2\pi G} = \frac{M_2^3 \sin^3 i}{(M_1 + M_2)^2} = \frac{q^3}{(1 + q)^2} M_1 \sin^3 i\,, \tag{1.16}$$

where $q = M_2/M_1$ is the mass ratio of secondary to primary. In case we can estimate inclination and mass of primary, we can solve this cubic equation to obtain mass ratio and thus the mass of secondary.

1.1.2 Roche model

For modeling of lightcurves, it is common to model the stars as surfaces of constant potential in the so-called Roche model. These potentials are then used as parameters in the model. We are mainly interested in their conversion to stellar radii as more standard parameters. Potential around the binary system in a corotating frame can be written as a sum of gravitational potentials of binary components approximated as point masses and potential of centrifugal force. If we choose the center of mass of the more massive star as origin using 1.2 we can obtain

$$\phi = -\frac{GM_1}{a}\left[\frac{a}{r} + q\left(\frac{a}{\sqrt{r^2 - 2ra\lambda + a^2}} - \frac{r\lambda}{a}\right) + \frac{r^2}{2a^2}(1+q)(1-\nu^2) + \frac{1}{2}\frac{q^2}{1+q}\right], \tag{1.17}$$

where r is the distance from the point of origin and λ, μ and ν are directional cosines for x, y and z components of $\mathbf{r}$. By dividing by the factor in front of the parentheses, we obtain dimensionless potential, which after shifting its zero point and abbreviating $\rho = r/a$ reaches the form of so-called Kopal potential

$$\Omega = \frac{1}{\rho} + q\left(\frac{1}{\sqrt{\rho^2 - 2\rho\lambda + 1}} - \rho\lambda\right) + \frac{\rho^2}{2}(1+q)(1-\nu^2). \tag{1.18}$$

In case of general elliptical orbit and star not rotating synchronously (but still coplanar) we need to use a more complicated form of potential Prša [2018].

$$\Omega = \frac{1}{\rho} + q\left(\frac{1}{\sqrt{\rho^2 - 2\rho\lambda\delta + \delta^2}} - \frac{\rho\lambda}{\delta^2}\right) + F^2\frac{\rho^2}{2}(1+q)(1-\nu^2), \tag{1.19}$$

where $\delta = r_{12}/a$ is th dimensionless instantaneous separation and F is stars synchronicity parameter defined as ratio of orbital and rotational periods $F_i = P/T_i$.

To obtain radius of componets from given surface potential it is easies to select $\lambda = 0$, $\nu = 1$ in equation coinciding with direction towards star's pole thus obtaining dimensionless polar radius ρ from equation

$$\Omega_1 = \frac{1}{\rho_{pole,1}} + \frac{q}{\sqrt{\delta^2 + \rho_{pole,1}^2}}. \tag{1.20}$$

To obtain parameters of second star we just need to use transformation

$$\Omega' = \frac{\Omega}{q} + \frac{q-1}{2q}, \qquad q' = \frac{1}{q} \tag{1.21}$$

and use the above equations.

Modeling of the lightcurves of well-detached systems generally results in fractional radii ρ_1, ρ_2 given we know the mass ratio q. Furthermore, if we use one passband photometry only, we can expect to obtain the inclination of the orbit and ratio of component's effective temperatures along the radii from the shape and depths of primary and secondary minima. From their relative duration and spacing in phase, it is possible to obtain eccentricity e and argument of periastron ω in joint fit. Generally, we can see modulation in light even in-between eclipses caused by ellipticity of components, reflection of light in between stellar surfaces towards the observer, and Doppler boosting tied to the finite speed of light. For more details, see the book Prša [2018].

1.2 Apsidal precession in binaries

In some cases, the above description is not precise enough. In close binary systems, we can observe effects given by the spatial distribution of mass of the stars and even relativistic correction to classical theory. If we consider only non-dissipative processes conserving angular momentum and energy, a change in orientation of the orbit in the orbital plane is possible for an isolated binary star. Such process is called apsidal precession and is given by the rate of change of longitudes of periastron $\dot{\omega}$. Consequently, we need to specify two kinds of the orbital period - sidereal period P_s relative to stars and anomalistic period P_a relative to pericenter crossing. For the anomalistic period, we have

$$P_a = P_s(1 + \frac{\dot{\omega}}{2\pi}). \tag{1.22}$$

The rate of precession is always positive; therefore, the orbit is slowly rotating in space in the same direction as the body orbits. We can define the period of precession as

$$U = \frac{2\pi}{\dot{\omega}} \tag{1.23}$$

which is the time it takes for the orbit to complete one full rotation. Apsidal precession in binaries can be split into two terms given by relativistic correction and correction due to the non-symmetric nature of stars as

$$\dot{\omega} = \dot{\omega}_{rel} + \dot{\omega}_N. \tag{1.24}$$

Relativistic contribution is given by well known formula (e.g. Gimenez [1985])

$$\dot{\omega}_{rel} = \left(\frac{2\pi}{P}\right)^{\frac{5}{3}} \frac{3\left[G(M_1 + M_2)\right]^{\frac{2}{3}}}{c^2(1-e^2)} = \frac{2\pi}{P}\frac{3G(M_1 + M_2)}{ac^2(1-e^2)}, \tag{1.25}$$

where c is the speed of light in a vacuum.

Precession caused by the nonspherical nature of stars due to rotation and tidal interactions is derived in Sterne [1939]. Frist correction is given by equation

$$\dot{\omega}_N = \frac{2\pi}{P}\left\{k_{2,1}\left(\frac{R_1}{a}\right)^5\left[15q\frac{1+\frac{3}{2}e^2+\frac{1}{8}e^4}{(1-e^2)^5} + (1+q)\left(\frac{P}{P_1}\right)^2\frac{1}{(1-e^2)^2}\right] + \right.$$
$$\left. +k_{2,2}\left(\frac{R_2}{a}\right)^5\left[15\frac{1}{q}\frac{1+\frac{3}{2}e^2+\frac{1}{8}e^4}{(1-e^2)^5} + \frac{1+q}{q}\left(\frac{P}{P_2}\right)^2\frac{1}{(1-e^2)^2}\right]\right\}, \tag{1.26}$$

where $k_{2,1}$, $k_{2,2}$ are numerical constants of the apsidal motion for primary and secondary given by mass distribution inside the stars. One can find expressions even for higher orders in R/a in literature. The values of constant k_2 can be given by the polytropic index

- $n = 0 \rightarrow k_2 = 0.75$ for homogeneous spheres ,

- $n < 1 \rightarrow k_2 > 0.260$ for neutron stars ,

- $n = 1.5 \rightarrow k_2 = 0.145$ for convective interior stars and light white dwarfs ,

- $n = 2 \rightarrow k_2 = 0.0741$,

- $n = 3 \rightarrow k_2 = 0.0144$ for radiative interior stars and heavy white dwarfs,

- $n = 4 \rightarrow k_2 = 0.0013$.

The value of this constant is decreasing as the mass concentrate more to the middle of the star and vanishes for point masses. For some cruder estimates in close binaries with synchronous rotation of both stars with small eccentricity, we can use the following simplification of formula 1.26

$$\dot{\omega}_N \approx \frac{2\pi}{P} \left[k_{2,1} \left(\frac{R_1}{a} \right)^5 (16q + 1) + k_{2,2} \left(\frac{R_2}{a} \right)^5 \frac{16 + q}{q} \right]. \qquad (1.27)$$

Finally, we can calculate the period of apsidal precession of the binary system consisting of two same stars. Inserting $R_1 = R_2 = R$, $k_{2,1} = k_{2,2} = k_2$ and $q = 1$, we get

$$\dot{\omega}_N = \frac{2\pi}{U} \approx \frac{2\pi}{P} 34 k_2 \left(\frac{R}{a} \right)^5 \rightarrow \frac{U}{P} \approx \left(\frac{a}{R} \right)^5 \qquad (1.28)$$

as an order of magnitude estimate. We can see that even for a relatively compact system with $R/a = 0.1$ and an orbital period of the order of one day, we get the apsidal period in hundreds of years.

Apsidal precession can be observed as a change of shape of radial velocity curve for eccentric orbit or as a change of timing of eclipses in the case of eclipsing binaries. The second method has lower bounds on the accuracy of the measurements compared to the instrumental errors and therefore is more common. In this case, we can observe periodic changes in observed times of centers of eclipses compared to the times calculated given linear ephemerid in the so-called O-C diagram. These differences can then be fitted to obtain the period of precession U, orbital eccentricity e and longitude of periastron ω_0 at given epoch T_0. We can do so either by predicting each eclipse using full computation via Kepler equation 1.4 or using the power series given in Giménez and García-Pelayo [1983], which can be further approximated up to e^2 and $(i - \frac{\pi}{2})^2$ for $\omega = \omega_0 + \dot{\omega}T$ as

$$T = T_0 + P_s E - \frac{eP_a}{2\pi}(2 + \cot^2 i)\cos\omega + \frac{e^2 P}{4\pi}(\frac{3}{2} + 2\cot^2 i)\sin 2\omega, \quad (1.29)$$

$$T = T_0 + P_s E + \frac{P_a}{2} + \frac{eP_a}{2\pi}(2 + \cot^2 i)\cos\omega + \frac{e^2 P}{4\pi}(\frac{3}{2} + 2\cot^2 i)\sin 2\omega. \quad (1.30)$$

1.3 Triple star systems

In order to be stable, triple star systems form into a so-called hierarchical structure. Such a system consists of an inner binary star and a third body orbiting around it. The third body is usually less massive and luminous. As a first approximation, we can describe the system as two nested Keplerian systems. The inner pair is orbiting on an elliptical orbits around its center of mass, and this center of mass forms another binary with the third star, where each orbit can be described via equations from chapter 1.1. In the case of radial velocities measurement, we need to fit both orbits simultaneously. In equation 1.8 we can for γ_{12} (velocity of the center of mass of the inner binary) use the equation again

$$\gamma_{12} = \gamma - K_{12}(\cos(\nu_3(t) + \omega_{12}) + e_3 \cos \omega_{12}), \qquad (1.31)$$

$$RV_3 = \gamma + K_3(\cos(\nu_3(t) + \omega_3) + e_3 \cos \omega_3), \qquad (1.32)$$

where e_3, K_3, K_{12}, ν_3, ω_{12}, ω_3 are parameters of the outer orbit. In case of sufficient orbital coverage, we can fit the residuals of radial velocities of the inner binary after the binary fit and get the solution in two steps.

In the case of eclipsing binary, we get periodic changes in the O-C diagram caused by differences in distance between binary and observer and the finite speed of light c – so-called LITE effect. From the orbital motion in chapter 1.1 we can derive an equation

$$T = T_0 + P_1 E + \frac{a_{12} \sin i_3}{c} \left(\frac{1 - e_3^2}{1 + e_3 \cos \nu_{12}} \sin(\nu_{12} + \omega_{12}) + e_3 \sin \omega_{12} \right) , \quad (1.33)$$

where a_{12} is the semimajor axis of the orbit of the center of mass of the inner binary around the center of mass of the triplet. We can consequently obtain the orbital period of the third body P_3, $a_{12} \sin i_3$, e_3, ω_{12}, T_0 by fitting, from which we can compute the mass function of the third body as

$$f(M_3) = \frac{(M_3 \sin i_3)^3}{(M_1 + M_2 + M_3)^2} = \frac{4\pi^2 (a_{12} \sin i_3)^3}{G P_3^2} . \quad (1.34)$$

We can see that from LITE and spectroscopy, we are unable to eliminate the factor $\sin i_3$, and for estimation of M_3, we need to get it elsewhere.

1.3.1 Dynamical effects

If we consider gravitational interaction between inner and outer pairs, we get more contributions to O-C diagrams for eclipsing binaries

- short-term perturbations with period P_1 given by the distortion of elliptical orbit under the gravity of the third body with relative amplitudes of the order $(\frac{P_1}{P_3})^2$ which is hard to observe,

- medium-term perturbations with period P_3 given by the change of orientation and intensity of distorting potential with relative amplitudes of the order $\frac{P_1}{P_3}$ which can be significant and adds up to LITE,

- long-term perturbations with characteristic period $\frac{P_3^2}{P_1}$ and relative amplitude up to 1 tied to the apsidal and nodal precession of the system and Kozai-Lidov cycles which can cause even significant changes in depths of the eclipses.

Precise description of these perturbation is rather complex and can be found for several more concrete cases in Soderhjelm [1975], Borkovits et al. [2003], Borkovits et al. [2011]. The problem is, at its core, similar to the Lunar theory. In general, first-order effects vanish if the orbits are coplanar and circular.

1.4 Multiple star systems origins and evolution

When a cloud of interstellar matter is compressed by the outer source below Jeans mass M_J it starts to collapse freely under its gravity. Because $M_J \propto 1/\sqrt{\rho}$, the cloud fragments into clumps and streams while collapsing. Such clumps

slowly became dense enough for outgoing thermal radiation to be reabsorbed, thus slowing the contraction and heating the material. These clumps became rotating protostars with protoplanetary discs. Protostar systems later evolve into stars with more surrounding bodies (low mass stars, brown dwarfs, planets) developed from the disc. In the case of low-mass clouds, the stellar formations end when most of the material is exhausted, usually forming a bound system – open cluster. Heavy clouds can give birth to massive stars of classes O, B, which have strong stellar winds and intense radiation that clears the interstellar material before most of it is able to collapse into smaller stars. Removing a substantial amount of mass from the system causes it to become an unbound O-B association.

Given the proximity and hierarchical nature of cloud fragmenting, it is not surprising that multiple star systems are born. However, these systems undergo dynamical evolution by gravitational interaction with other nearby stars and each other. We can divide the systems into two categories

- *hierarchical systems* where orbits of stars form a hierarchical binary structure with sufficient space between orbits,

- *Trapez systems* where the distances between any stars are comparable and motion is chaotic.

Trapez type of multiple star system decays at a time scale of about a few thousand years. For the hierarchical system to be stable, some separation between orbits given by the ratio of orbital periods must be fulfilled. As an example the empirical result by Tokovinin [2007] states

$$\frac{P_3}{P_1} \geq \frac{5}{(1 - e_3)^3} \, . \tag{1.35}$$

1.4.1 Dynamical evolution & nonconservative processes

In the long-term evolution of the stellar system, the effect of energy dissipation by tidal interaction has an important role. The gravitational force of one body acting on the other gives rise to tidal bulges - deformation of the shape of the star - which move according to disturbing force. The energy is then converted to heat by viscous forces inside the body, thus arising the name of the process - tidal friction. In general, the decrease of the system's total energy implies deepening the potential well, thus decreasing the system's dimensions and shortening the orbital period. Furthermore, these processes conserve the stellar system's total angular momentum but can transfer angular momentum between stars and between different modes of motion (rotation, orbit).

In isolated binaries, the orbits are circularised by tidal interaction on a time scale given by Tassoul [1988]

$$\frac{\tau_{circ}}{\text{year}} = \frac{14.4 \times 10^{-N/4}}{(1 + q)^{11/8} r_g^2} \left(\frac{L_1}{L_\odot} \right)^{-1/4} \left(\frac{M_1}{M_\odot} \right)^{-1/8} \left(\frac{R_1}{R_\odot} \right)^{9/8} \left(\frac{a}{R_1} \right)^{49/8} , \tag{1.36}$$

where he considered binary star where rotational angular momentum is negligible in compared to total angular momentum, the orbit is close to circular, the secondary is treated as a point mass, and mass loss by wind is neglected. Parameter r_g is fractional gyration radius describing mass distribution inside the

star (numerical coefficient for computation of momentum of inertia), and N is a numerical factor describing energy disipation efficiency in a turbulent layer of the stellar atmosphere. For early type stars we can take $N = 0$ and $r_g = 0.1$ and for solar type and later stars we can take $N = 10$ and $r_g = 0.2$. He further argues that allowing the second body to be a real star would just add a numerical factor close to unity.

There is also a tendency to synchronize rotational T_1, T_2 and orbital P periods of stars giving rise to synchronous rotation $T_1 = T_2 = P$ on a timescale given by Tassoul [1987]

$$\frac{\tau_{synchr}}{\text{year}} = \frac{14.4 \times 10^{-N/4}}{q(1+q)^{3/8}} \left(\frac{L}{L_\odot}\right)^{-1/4} \left(\frac{M}{M_\odot}\right)^{-1/8} \left(\frac{R}{R_\odot}\right)^{9/8} \left(\frac{a}{R}\right)^{33/8}. \tag{1.37}$$

In the case of an eccentric orbit, the tidal forces are the strongest at the periastron therefore the angular velocity of orbital and rotational motion are closer to coinciding at the periastron, and the synchronized period approaches

$$T = P\frac{\sqrt{1-e}^3}{\sqrt{1+e}} < P. \tag{1.38}$$

1.4.2 Kozai cycles with tidal friction

It is a well-known result of work by Kozai, Lidov, and others that in three-body systems, there occur oscillations in the eccentricity of inner orbit e_{12} and relative inclination I of inner and outer orbit known as Kozai cycles. During the oscillations, the quantity known as Kozai invariant

$$\Psi = (1 - e_{12})^2 \cos^2 I \tag{1.39}$$

is conserved due to the conservation of projection of inner orbit's angular momentum in the normal direction of outer orbit. The oscillation amplitude is independent of the mass of the third body or its separation from the central binary. The period of these oscillations is given by

$$\tau_{Kozai} = \frac{2}{3\pi} \frac{P_3^2}{P_1} \frac{M_1 + M_2 + M_3}{M_3} (1 - e_3^2)^{\frac{3}{2}}. \tag{1.40}$$

As we discussed previously, in close encounters, the tidal forces start to play an important role. Kozai cycles can induce tidal friction even from an initially circular orbit in part of the cycle with high eccentricity. The inner orbit will thus slowly shrink, and the outer orbit will expand due to the conservation of total angular momentum. The period of oscillations thus becomes larger, and the process will be suppressed by the precession of the periastron by other sources (binary tidal interaction, general relativity) or stopped altogether by the expulsion of the outer body from the system. The system will be locked to a high eccentricity orbit that will slowly dissipate by binary tidal interaction arriving at the final close circular orbit. The energy dissipation is strongest during high eccentricities, so the minimal inclination during cycles is nearly conserved and becomes the final mutual inclination of the orbits. Kozai cycles with tidal friction thus produce overpopulation of triple star systems with close binaries with periods of

the order of days and with mutual orbit inclinations around 40° and 140° as can be seen in the work of Fabrycky and Tremaine [2007] via evolutional simulation of triple systems that resulted in the distribution of relative inclinations and periods given in figure 1.1. Interesting case studies for various triple systems were done, for example, work on λ Tau and β Per by Kiseleva et al. [1998]. These studies bring theoretical background for observational studies, for example, by Tokovinin et al. [2006] suggesting that all binaries with comparable masses of components and of periods $P < 5\,\mathrm{d}$ are actually part of triple systems.

Figure 1.1: Triple systems after Kozai evolution - Fabrycky and Tremaine [2007]
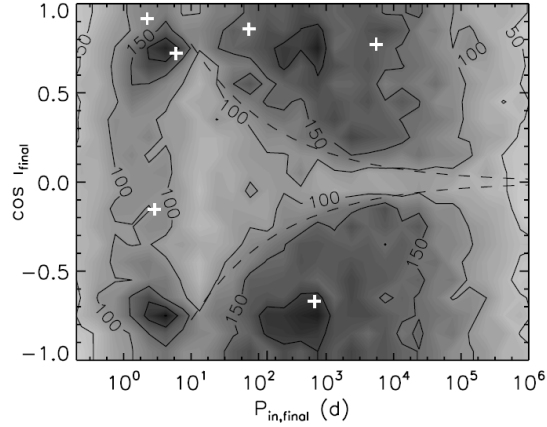
Two-dimensional histogram of the cosine of the final mutual inclination of inner and outer binaries vs. the final inner binary period. The region between the dashed lines corresponds to the initial values of systems that may lose enough angular momentum by Kozai cycles, and enough orbital energy by tidal friction, to circularize to final periods less than ten days.

2. Methods and data

2.1 Spectroscopy

We were working with archival spectra from Ondřejov Observatory made using equatorial mounted $2\,\mathrm{m}$ $f/4.5$ Perek telescope with coudé single order spectrograph. The spectra were taken in its first order in red spectral region around Hα line with resolving power about $13\,000$ on liquid nitrogen cooled CCD camera. The projected slit size is just $0.6\,\mathrm{arcsec}$ which lies under the usual seeing. Spectrum extraction and wavelength calibration against thorium-argon lamp was carried out by M. Šlechta; a list of observers is provided per target in later chapters. More information on telescope and spectrograph is available on webpages of observatory `https://stelweb.asu.cas.cz/en/telescope/`.

These spectra were rectified and converted from *.fits* to *.ascii* by the software `reSPEFO` developed by Adam Harmanec available as *.jar* archive at `https://astro.troja.mff.cuni.cz/projects/respefo`. For quick introduction to the software see the appendix C of article Harmanec et al. [2020].

2.1.1 `KOREL` disentangling

We aim to obtain radial velocity curves and spectra of components of the binaries and look for third bodies in residuals. For spectral disentangling was used software `KOREL` Škoda and Hadrava [2010], Škoda et al. [2012] provided via a virtual observatory available at `https://stelweb.asu.cas.cz/vo-korel/`. The method is based on the idea that set Φ_i of spectra of multiple star system can be viewed as a linear combination of spectra of its constituents Φ^A Doppler shifted by their orbital motion represented as convolution with appropriate Dirac delta function

$$\Phi_i(x) = \Phi^A(x) * \delta(x - v_i^A) + \Phi^B(x) * \delta(x - v_i^B) + \dots \tag{2.1}$$

This can be transformed by Fourier transform to the form

$$\phi_i(y) = \phi^A(y)\exp(iyv_i^A) + \phi^B(y)\exp(iyv_i^B) + \dots \tag{2.2}$$

which can be viewed for a given y as a simple matrix equation for i from one to the number of obtained spectra N where we multiply the M transformed spectra of components by $N \times M$ matrix given by shifts to obtain transformed observed spectra. The shift matrix is furthermore constrained by orbital motion and is, therefore, a function of orbital parameters. The spectra of components thus can be obtained from measured spectra solving the inverse problem for the shift matrix. As the problem is overdetermined, our goal is to find the correct orbital solution, which will result in minimal residual of transformed spectra. This optimization is implemented via the simplex method. Further information on the process of disentangling and the mathematics behind it can be found in the guide Hadrava [2004].

To use `KOREL` we need to prepare our spectra. Firstly we have prepared the list of filenames and times of observation and calculated signal to noise ratio of the spectra using the `SN2` and `SNVAHY` programs by P. Harmanec on spectral range

$3700\,\text{Å} - 3720\,\text{Å}$ to obtain *prekor.lst* file. Than we use program `HEC35D` by P. Harmanec to create input data file for `KOREL` *korel.dat*. This program provides rebinning of the spectra in wavelength scale to scale equidistant in radial velocities and correct formating to run under `KOREL`. The programs, as well as the user's manual, can be found at `https://astro.troja.mff.cuni.cz/ftp/hec/HEC35`. We have created to *korel.dat* files

- "stellar" with wavelength range $6335\,\text{Å} - 6776\,\text{Å}$ with a step of $2.6\,\text{km/s}$ containing stellar spectral lines and telluric lines of atmospheric water vapor,

- "telluric" with range $6440\,\text{Å} - 6530\,\text{Å}$ with the same step dominated by water vapor lines and only week stellar lines.

Now we can proceed to the disentangling. We are going to disentangle to obtain tree spectra - of the two components of the binary and of the telluric lines. Telluric lines have variable strength according to atmospheric conditions (this is the reason why we discarded spectral region $6268\,\text{Å} - 6335\,\text{Å}$ containing telluric lines of oxygen with line strength varying independently from those of water vapor). The movement of telluric lines is modeled as a third body in the system orbiting the center of mass of the binary without causing its movement by selecting appropriate semiaplitude (sufficiently small, we use 0.001), Earth's orbital period, eccentricity, and mass ratio (such that K2 parameter is equal to the semiaplitude of heliocentric corrections) and argument of periastron of the outer orbit. The last two parameters are given by the position of our binary on the sky as a projection of Earth's orbital motion and can be computed exactly or approximately guessed and fitted. We are going to use control keys `1 1 0 0 2 1 0 2 60` which prompt `KOREL` to further generate files of spectral residuals *korel.o-c* and initial estimates of orbital parameters in *korel.par* file.

For our first run of `KOREL` we use the "telluric" datafile to solve for the strength of telluric lines and optionally improve on their orbit using fixed orbital parameters of the binary. Obtained strengths from *korel.res* are then transported to *korel.par*. Now we can disentangle our binary using "stellar" datafile with fixed strength of telluric lines and their orbit. We also fixed the orbital period, eccentricity, argument of periastron, and rate of periastron precession using published values from photometric studies and selecting the initial time of periastron passage as the epoch of photometric ephemerid. Thus we obtained the amplitude of radial velocities, mass ratio, and time of periastron passage. As a next step, we run `KOREL` using these values as initial estimates and also allowing eccentricity and argument of periastron to be fitted. As a result, we obtain *korel.res* file containing orbital elements and measured radial velocities of binary, *korel.spe* file containing spectra of binary components and telluric lines and *korel.o-c* file containing spectral residuals. Obtained spectra of binary were rectified in `reSPEFO` for later use.

As a next step, we attempted to obtain spectra of possible third bodies in the system. To consider the attempt feasible, we first constructed the mean of spectral residuals and compared them to expected values derived from signal to noise ratio of spectra on hand. In case significant structures were present, we try to disentangle the additional spectra of the third body on smaller spectral intervals (for more controllable runs) using published orbits of the third body from

the LITE effect if available or as a static body in binary reference frame otherwise. In spectral regions without telluric lines or lines from binary, we disabled the according contribution to spectra in *korel.par* to ease the disentangling. Spectra from all regions were then rectified and sewn together.

2.2 TESS photometry

Transiting Exoplanet Survey Satellite is photometric observatory by NASA orbiting Earth on highly eccentric orbit with orbital period 13.7 d equipped with four $24° \times 24°$ wide-field cameras in 4×1 configuration. Each camera has 105 mm aperture, focal ratio of $f/1.4$, and spatial resolution of about half arc-minute. The detector has quite a broad bandpass $6000\,\text{Å} - 10\,000\,\text{Å}$. The survey covers parts of the sky by sectors that are observed continuously during two consecutive orbits with the exception of time around perigee used for data downlink. We will be using data with a two-minute cadence. More information about the observatory can be found at `https://heasarc.gsfc.nasa.gov/docs/tess/` and in the TESS Instrument Handbook by Vanderspek et al. [2018]. We were using lightcurve downloaded from Mikulski Archive for Space Telescopes `https://archive.stsci.edu/missions-and-data/tess` generated by SPOC pipeline by Jenkins et al. [2016]. The lightcurve was first extracted from *.fits* to a free formatted file containing times and fluxes by `fv` FITS Viewer available for free at `https://heasarc.gsfc.nasa.gov/ftools/fv/`.

2.2.1 `PHOEBE` lightcurve fitting

For modeling of lightcurve, we have used software `PHOEBE` developed by Andrej Prša, which is freely available at `http://phoebe-project.org/` with its Windows operable legacy version `PHOEBE 1.0`. The problem of eclipsing binary stars modeling is described in detail in the book by Prša [2018], the software in manual by Prša and Harmanec [2010] and practical guide by Zasche [2016] wich we are going to loosely follow.

The only star with available TESS photometry from our set so far is BW Boo. We were modeling a full month-long lightcurve as well as a subset consisting of two consecutive primary minima and data in-between with the Johnson R filter selected as a proxy to TESS passband. We select detached binary fitting mode and insert the orbital period, mass ratio, semimajor axis, and primary star effective temperature from earlier works, as well as left synchronicity parameters, albedos, and gravity brightenings at default values. We proceed with the calculation of luminosities and approximate fit-up of time of origin, initial eccentricity, and argument of perihelion by hand. Then we proceed in steps first fitting for t_0, e, ω, then for inclination i, secondary star effective temperature T_2, and surface potentials Ω_1 and Ω_2. Then we interpolated the limb darkening coefficients using logarithmic law and `PHOEBE` tables and consequently fit for both groups of parameters simultaneously with few iterations updating the limb darkening coefficients between iterations. Next we choose finer description of star mesh going from $20 \times 20/5 \times 5$ mesh to $35 \times 35/15 \times 15$ mesh. If the data allowed it, we fitted for albedos also. We note that obtaining only crude estimates of albedos was

possible because of some long-term variability correlated with the subpixel movement of the target along with the detector. In our case, fitting for synchronicity parameters was not necessary due to quite a big orbital and rotational periods presenting as narrow spectral lines. Finally, we tried to fit the third light also. Because of extremely slow changes in third light value between iterations (though moving monotonically), we also attempted the whole process with initially fixed nonzero third light consistent with KOREL spectral solution. The subset of data was then used to judge the uncertainty of obtained values. Finally, we recovered the usual parameters of stars from equations presented in chapter 1.1.

3. Stellar systems under investigation

3.1 V335 Serpentis

V335 Serpentis (HD 143213, SAO 121294, TYC 353-301-1) is a variable star of magnitude about 7.5^m discovered to be a variable by the Hipparchos satellite survey with a possible eclipse depth of about 0.7^m Makarov et al. [1994]. Using Hipparchos photometry together with their own visual estimates Bastian and Born [1997] and Bastian and Born [1998] the star was classified as Algol type eclipsing variable with a period about $P = 3.45$ d. Later works by Bozkurt [2011] and Lacy et al. [2012] used both new photometric and double-line spectroscopic observations using a total of about 80 spectra to arrive at the classification of components as A1 and A3 stars slightly evolved from the main sequence at a distance of about $d = 200$ pc. Gaia Collaboration [2020] has determined the parallax of $\pi = (5.16 \pm 0.03)$ mas giving the distance of $d = (193.9 \pm 1.1)$ pc. The parameters of components and their orbit according to these works can be found in table 3.1.

We have in our disposal 33 spectra taken between years $2005 - 2013$ by following observers: M. Wolf (14), J. Sloup (10), M. Tlamicha (9), L. Kotková, L. Řezba, M. Šlechta (6), D. Korčáková, P. Zasche (5), J. Fuchs, P. Harmanec, P. Mayer (2) and A. Avdibegović, L. Bartík, P. Bystřický, I. Kotíková, J. Kubát, B. Kučerová, J. Nemravová, M. Netolický, L. Pilarčík, J. Schovancová, V. Sochora, P. Švaříček, P. Svoboda, M. Tukinská and M. Zejda (1). The mean signal-to-noise ratio of spectra is about $S/N = 200$. Given the number and precision of measured radial velocities in Lacy et al. [2012], the elements in table 3.1 were used as initial parameters and we allowed the convergence of T_0, e, ω, K_1 and q. We have disentangled the spectra of two components and telluric lines. The resulting spectra of components normalized to the common continuum can be seen in figure 3.1 together with the mean residual of the spectra. We can see that the residuals are in absolute value smaller than 0.001 with a standard deviation of about 0.00024.

Table 3.1: Constituents and orbit of V335 Ser according to Lacy et al. [2012]

T_0 (periastron)	$(2\,455\,492.7960 \pm 0.0052)$ d	
P_s	$(3.449\,883\,7 \pm 0.000\,001\,2)$ d	
a	(15.324 ± 0.028) R$_\odot$	
q	0.888 ± 0.003	
e	0.1408 ± 0.0009	
ω_0	$(65.2 \pm 0.4)°$	
$\dot{\omega}$	$(0.41 \pm 0.16)°$/y	
i	$(87.19 \pm 0.15)°$	
R	(2.03 ± 0.03) R$_\odot$	(1.73 ± 0.04) R$_\odot$
M	(2.147 ± 0.014) M$_\odot$	(1.906 ± 0.008) M$_\odot$
T_{eff}	(9020 ± 150) K	(8510 ± 150) K
L	(24.5 ± 1.8) L$_\odot$	(14.1 ± 1.5) L$_\odot$

Table 3.2: Spectroscopic elements of V335 Ser derived via KOREL

element	our work	Lacy et al. [2012]
P_s	3.449 883 7 d (fixed)	
T_0 (periastron)	2 455 492.802 d	$(2\,455\,492.7960 \pm 0.0052)$ d
e	0.1391	0.1411 ± 0.0013
ω_0	66.2°	$(65.28 \pm 0.57)°$
K_1	106.13 km/s	(106.57 ± 0.12) km/s
q	0.8859	0.8876 ± 0.0030

Measured radial velocities via KOREL are presented in the table A.2 in the appendix A and plotted in the figure 3.2. Obtained orbital elements of KOREL fit can be found in table 3.2. Measured values of radial velocities are consistent with the solution by Lacy et al. [2012]. The two-body model has mean residuals of about $1.0\,\text{km/s} - 1.5\,\text{km/s}$ which are standard when using the Ondřejov linear spectra.

Figure 3.1: Disentangled spectra of components of V335 Serpentis
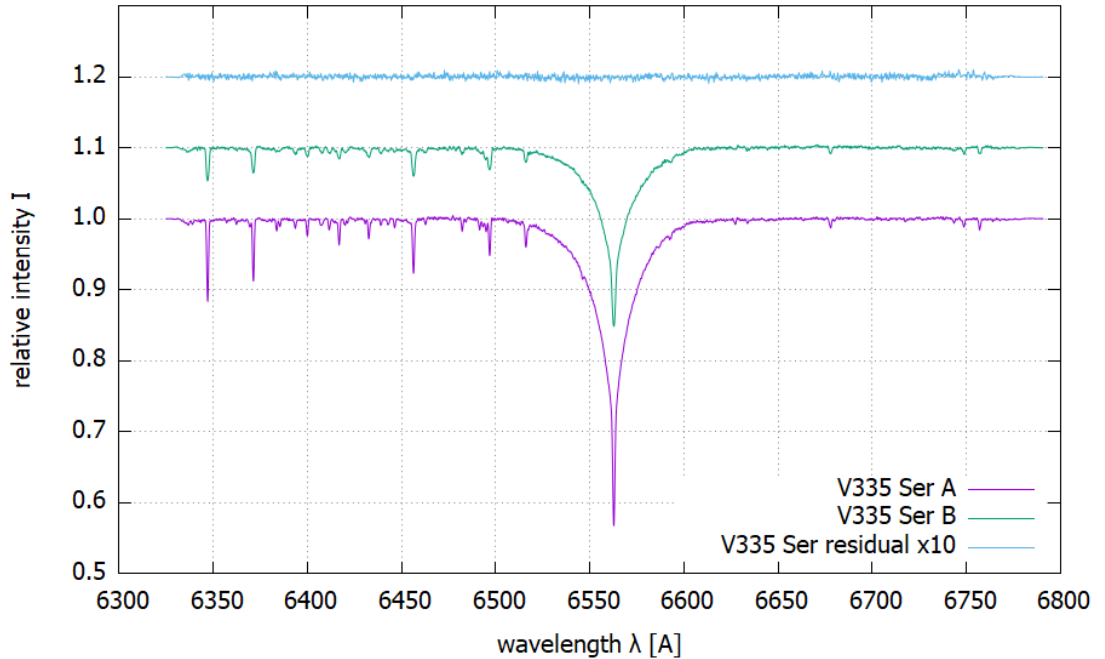
From bottom to top: spectrum of brighter component A, spectrum of component B shifted by 0.1 upwards, mean residual of spectra magnified by factor of 10 shifted by 1.2 upwards. Spectra of components are normalized to the common continuum level.

Spectra of both components contain the lines of hydrogen Hα, lines of singly ionized silicon SiII at $\lambda = 6347\,\text{Å} \,\&\, 6371\,\text{Å}$, lines of ionized iron FeII at $\lambda = 6417\,\text{Å}, 6456\,\text{Å}, 6516\,\text{Å}$ and lines of other heavier elements. The lines of helium are not present, suggesting the spectral classification of both components as early A stars in accordance with previous publications. The full-width of metallic spectral lines is under $2\,\text{Å}$ which is comparable with the observed full-width of disentangled telluric lines and is thus the limit of spectral resolution given by the spectrograph and detector. We note that spectral lines of secondary seem to

Figure 3.2: Radial velocities of V335 Serpentis in binary reference frame
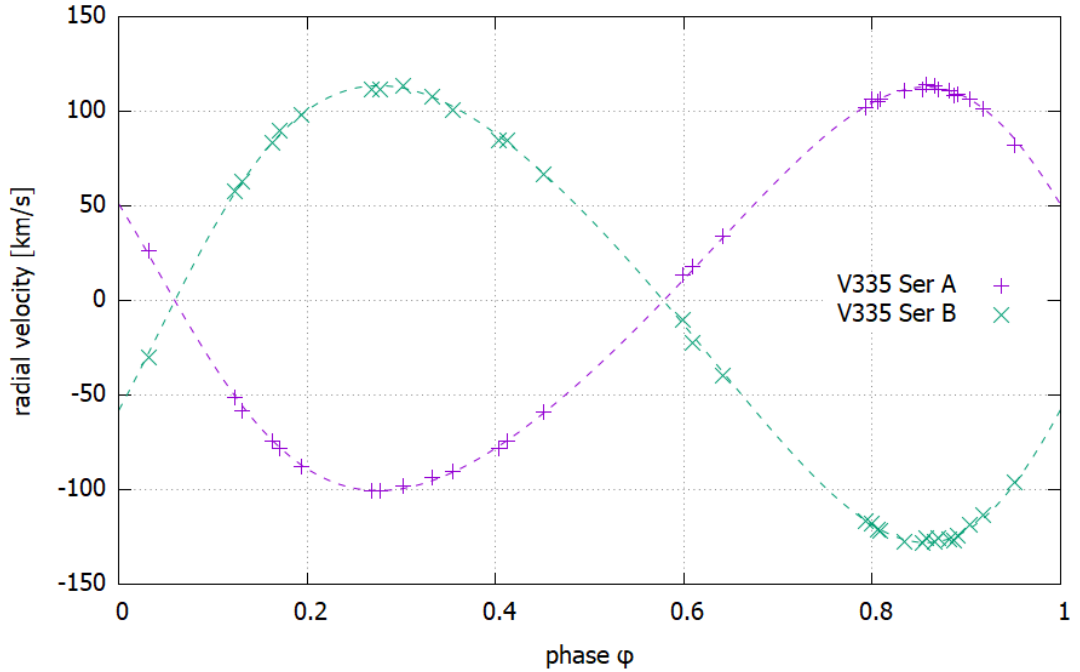
V335 Ser exhibits visibly eccentric RV diagram, standard deviation of one measurement from the model is 1.14 km/s for component A and 1.40 km/s for component B. Stability of wavelength calibration given by the dispersion of telluric lines is about 0.80 km/s.

be slightly narrower under the width of 1.5 Å. We can therefore limit rotational velocity of primary star by $v_A \approx v_A \sin i < 35$ km/s and secondary by $v_B \approx v_B \sin i < 50$ km/s limiting their rotational periods by $P_A > 2.9$ d and $P_B > 1.9$ d respectively. Therefore tidally locked synchronized rotational periods are possible.

The residual of the spectra suggests the binary is without another component. If we consider a possible third body in the system with at least some spectral lines of intensity 0.1, when normalized on itself, we arrive at a quite relaxed limit of 1:100 in red filter luminosities between this body and the whole system. Using tables of absolute magnitudes and color indices of main sequence stars, for example, by Pickles [1998], we arrive at the conclusion that a possible companion needs to be of a later spectral class than about K1. If we consider a more stringent limit of 1:300 given by the amplitudes of changes in a slightly binned spectrum, we arrive at spectral class no earlier than K4. The only possible main sequence companion is, therefore, a late K or M dwarf.

3.2 BW Bootis

The variable star BW Boo (HD 128661, SAO 64240, TYC 2560-693-1) was identified to be probable 7.1^m eclipsing binary by Jackisch [1968]. Later Gorza and Heard [1969] measured single line radial velocities and constructed the first orbit of the system with an orbital period of $P = 3.33$ d. Kurpinska [1975] obtained the first photoelectric light curve of the variable. Later work was concentrated on collecting times of minima of the variable. The first comprehensive study was done by Glazunova [2011] using Hipparchos photometry alongside the Kurpinska [1975] photometry and two echelle spectra. She observed the spectra of both components close to elongation and obtained pair of radial velocities and spectra yielding the spectral classification of components as A2Vm and G6. The secondary component spectra has lithium lines present, identifying it as a T Tauri star. Published parameters of components and orbit can be found in table 3.3. The distance to the system according to Gaia Collaboration [2020] parallax $\pi = (6.82 \pm 0.07)$ mas is $d = (146.6 \pm 1.5)$ pc.

We have used 21 spectra taken between the years 2007 and 2017 with a mean signal-to-noise ratio of about $S/N = 200$. Observation were carried out by P. Zasche (11), L. Řezba (10), M. Wolf (7), J. Sloup, M. Tlamicha (4), J. Fuchs, J. Polster (3), L. Kotková, M. Šlechta (2), P. Bystrický, I. Kotíková, P. Rutsch, V. Sochora, M. Zejda (1). First, we attempted the binary star disentanglement using published orbital parameters, allowing the fit of K_1 and q. Then we relaxed all orbital parameters obtaining spectroscopic elements in table 3.4. The resulting mean residual spectra contained a dip of about 0.003 near Hα; we, therefore, proceed to the disentanglement of the three-body system with all orbital elements fixed. We used previous orbital parameters of binary, and the third body was assumed to be stationary. Obtained spectra of components can be seen in figure 3.3. Measured radial velocities of all spectral components in three body model can be found in table A.1 in appendix A. The radial velocity diagram for binary can be seen in figure 3.4, diagram of radial velocities of the center of mass of the binary system and the third body can be seen in figure 3.5.

The spectrum of the component A contains the line of hydrogen Hα, singly ionized iron FeII at $\lambda = 6417$ Å, 6456 Å, 6516 Å, ionized silicon SiII at $\lambda = 6347$ Å & 6371 Å, and lines of other heavier elements with lines of helium absent wich is consistent with classification as an early A star. The spectrum of secondary and tertiary contain the line of hydrogen Hα and many lines of neutral metals in intensity comparable to G class stars. Full-width of metallic spectral lines of primary and secondary is about 1.5 Å which is similar to the width of disentangled telluric lines. We can limit the rotational velocity of the stars by about $v \approx v \sin i < 35$ km/s and rotational periods by $P_A > 2.5$ d, $P_B > 1.5$ d. Synchronous rotation of components is possible. In the case of the third component, we did not recover lines of metals with good quality; in general, the line-like features seem to be broader with widths of about ≈ 3 Å. We note that Hα line is, in comparison with component B, narrower at the top and wider at the bottom and of about 3/4 intensity.

We proceeded to fit available TESS photometry in `PHOEBE`. We attempted to fit for the third light, but this parameter's convergence was rather slow and nonproductive. Therefore, we present two different solutions for the lightcurve

Table 3.3: Constituents and orbit of BW Boo according to Glazunova [2011]

|	
T_0 (primary eclipse)	$2\,440\,362.9026\,\mathrm{d}^{\dagger}$
P_s	$3.332\,821\,\mathrm{d}^{\dagger}$
a	$13.67\,\mathrm{R_{\odot}}$
q	0.56
e	0.140 ± 0.002
ω_0	$(166 \pm 2)^{\circ}$
i	$(81.4 \pm 0.6)^{\circ}$
R	$(1.9 \pm 0.4)\,\mathrm{R_{\odot}}$ $1.2\,\mathrm{R_{\odot}}$
M	$(2.0 \pm 0.1)\,\mathrm{M_{\odot}}$ $1.1\,\mathrm{M_{\odot}}$
T_{eff}	$8900\,\mathrm{K}$ $5550\,\mathrm{K}$
L	$21.62\,\mathrm{L_{\odot}}$ $1.24\,\mathrm{L_{\odot}}$

† by Kurpinska [1975], it should be noted that Glazunova [2011] did not provide linear ephemerid and thus phase extrapolated to present day has accuracy of order of 0.01.

Table 3.4: Spectroscopic elements of BW Boo derived via `KOREL` binary solution

element	our work
P_s	$3.332\,82\,\mathrm{d}$ (fixed)
T_0 (periastron)	$2\,454\,214.6454\,\mathrm{d}$
e	0.1358
ω_0	165.27°
K_1	$73.46\,\mathrm{km/s}$
q	0.5620

Figure 3.3: Disentangled spectra of components of BW Bootis
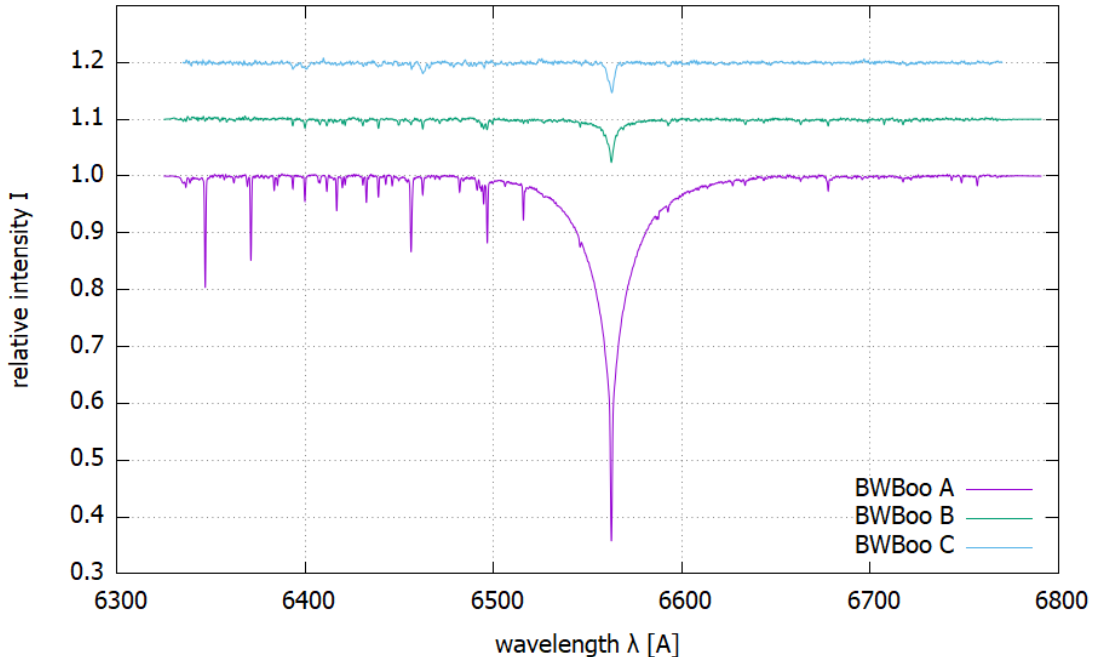
From bottom to top: spectrum of component A, spectrum of dimmer component B shifted by 0.1 upwards, spectrum of component C shifted by 0.2 upwards. Spectra of components are normalized to the common continuum level.

with fixed third light values at $l_3 = 0\%$ and $l_3 = 15\%$, which is around the upper estimate for the contribution of the third body visible in decomposed spectra. Errors of the parameters were estimated by running the fitting procedure multiple times and on subsets of the full dataset. Final estimates of the fit parameters can be found in table 3.5. Lightcurve of the system together with fit residuals can be seen in figure 3.6.

Finally, we computed the orbital parameters of the binary and physical parameters of the components of the system using the equations in chapter 1.1 presented in table 3.6. We accepted the value of eccentricity and argument of periastron from photometric fit as we deem this method more suitable for its precise and accurate estimation. The error in radial velocity semiamplitude was estimated as a root mean square error of one RV measurement divided by the square root of the number of observations to be about $\Delta K_1 = 0.3\,\mathrm{km/s}$ and similarly for mass ratio $\Delta q \approx \Delta K_1 \sqrt{2} q / K_1 = 0.003$. We note that compared to Glazunova [2011] we obtained components that are closer to each other in terms of radii and effective temperatures.

The third body in the system is strongly suggested only by the spectral feature on the Hα line in the disentanglement. This possible G class companion seems to be on a common orbit with the eclipsing pair as suggested by figure 3.5. We can see changes in radial velocities of the center of mass of the binary and the third body in opposite directions. Possible orbital period of this motion is about $P_3 \approx 3000\,\mathrm{d}$. Semiamplitude of radial velocities of the third component seems to be about $K_3 \approx 5\,\mathrm{km/s}$, for the center of mass about $K_{12} = 2\,\mathrm{km/s}$ which is consistent with the expected mass ratio of about $q_3 \approx 0.3$ estimated from the spectral classes of the components. The value of the amplitude itself is

Figure 3.4: Radial velocity diagram of central binary of BW Boo in binary reference frame
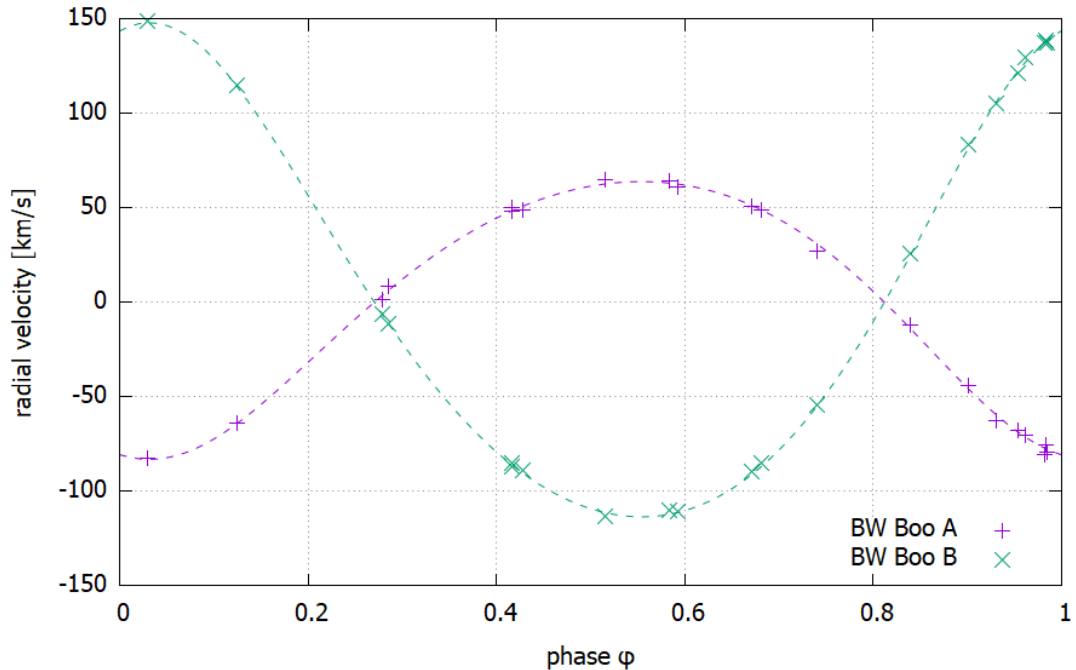

BW Boo exhibits visibly eccentric RV diagram, standard deviation of one measurement from the binary model is 1.88 km/s for component A and 1.08 km/s for component B. Stability of wavelength calibration given by dispersion of telluric lines is about 0.98 km/s.

Table 3.5: Photometric fit parameters using `PHOEBE`

| l_3	15% (fixed)	0% (fixed)
ω	$(163.1 \pm 0.3)°$	
e	0.1424 ± 0.0003	
i	$(82.35 \pm 0.05)°$	$(81.68 \pm 0.02)°$
T_1	8900 K (fixed)	
T_2	$(6380 \pm 20)\,\text{K}$	$(6450 \pm 5)\,\text{K}$
Ω_1	8.80 ± 0.03	8.49 ± 0.02
Ω_2	6.90 ± 0.03	

consistent with the estimated masses and orbital period of the third body, yielding moderate inclinations. The orbit also seems to be eccentric. More data is needed to confirm these claims; for example, analysis of eclipse timing variation can lead to confirmation of the orbit and its more precise characterization. Another option is to try to fit for the third light in the lightcurve model using a multicolor observation that can help with the apparent degeneracy of the fit in this parameter or obtain precise radial velocities from the metallic spectral lines of the primary that are suitable for such venture.

Figure 3.5: Radial velocity of the center of mass of the binary component and tentative third body in the system of BW Boo
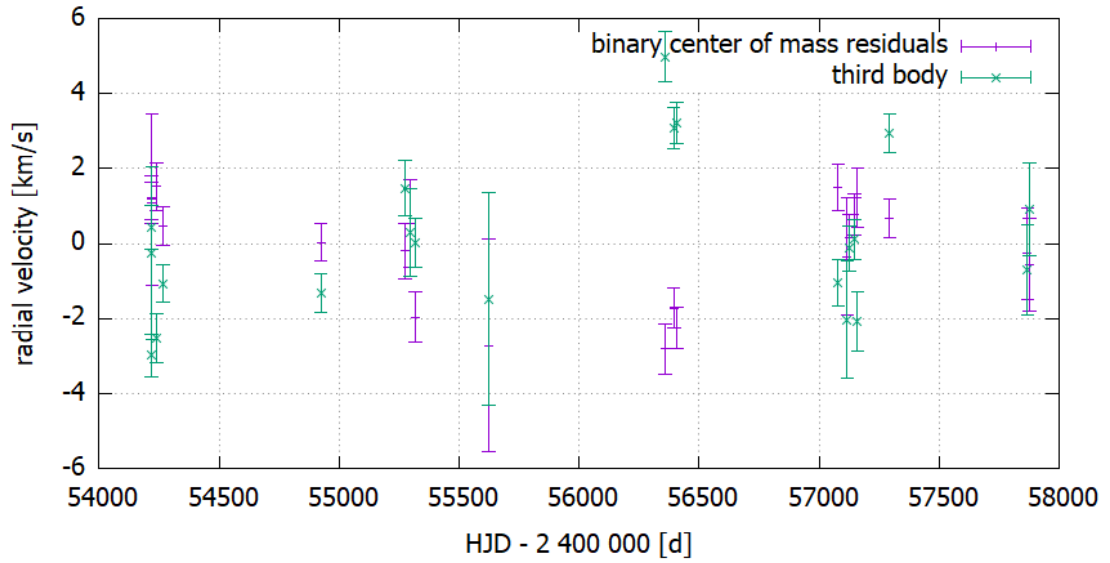
After correction by residuals of the radial velocity of telluric lines, we see a possible dynamical connection between the bodies. We note that there can be a different constant shift in the radial velocities for the two curves as the `KOREL` measures only relative changes in radial motion.

Figure 3.6: Lightcurve of the system BW Boo from TESS survey
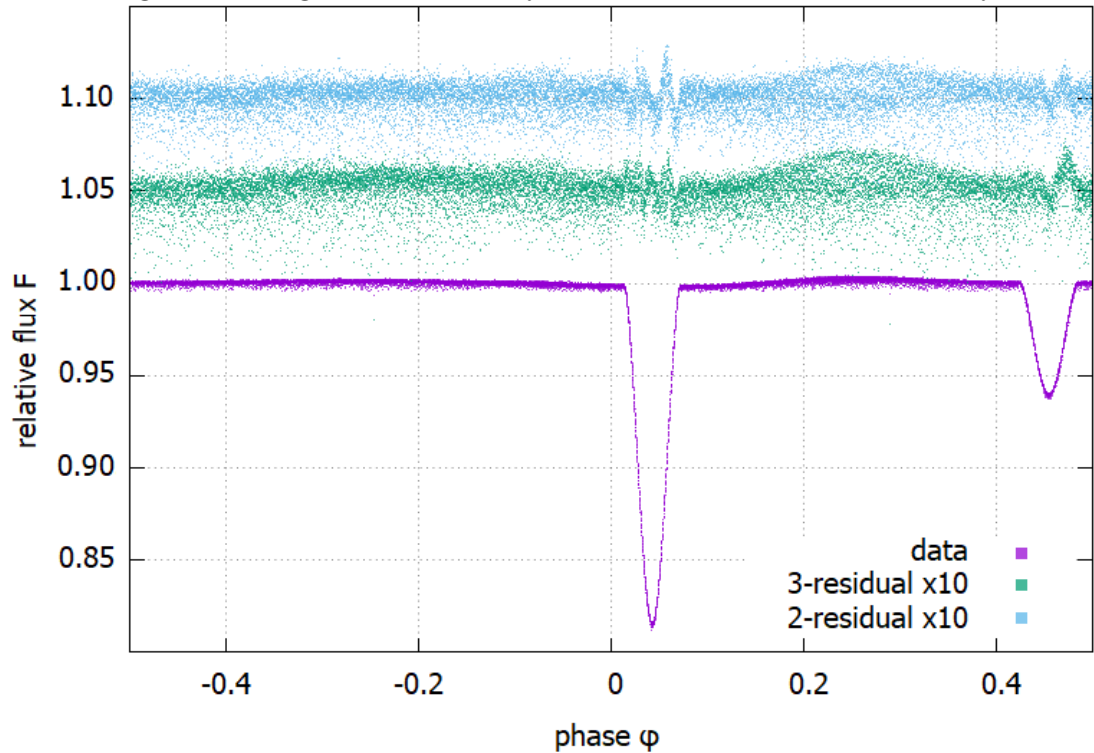
Bottom: phased TESS lightcurve, middle: residuals of the model with third light at 15%, top: residuals of the model without the third light. We can see there is no significant difference between the quality of these models.

Table 3.6: Constituents and orbit of central binary of BW Boo - our work

	triple star solution	double star solution
T_0 (primary eclipse)	$(2\,458\,943.3614 \pm 0.0001)\,\mathrm{d}$	
T_0 (periastron)	$(2\,458\,943.898 \pm 0.002)\,\mathrm{d}$	
P_s	$3.332\,821\,\mathrm{d}$ (fixed)	
a	$(13.43 \pm 0.07)\,\mathrm{R_\odot}$	
q	0.562 ± 0.003	
e	0.1424 ± 0.0003	
ω_0	$(163.1 \pm 0.3)°$	
i	$(82.35 \pm 0.05)°$	$(81.68 \pm 0.02)°$
R_1	$(1.648 \pm 0.007)\,\mathrm{R_\odot}$	$(1.712 \pm 0.006)\,\mathrm{R_\odot}$
R_2	$(1.363 \pm 0.013)\,\mathrm{R_\odot}$	
M_1	$(1.87 \pm 0.03)\,\mathrm{M_\odot}$	
M_2	$(1.05 \pm 0.02)\,\mathrm{M_\odot}$	
$T_{\mathrm{eff},1}$	$8900\,\mathrm{K}$ (fixed)	
$T_{\mathrm{eff},2}$	$(6380 \pm 20)\,\mathrm{K}$	$(6450 \pm 5)\,\mathrm{K}$

3.3   DR Vulpeculae

DR Vulpeculae (HD 339770, SAO 88380, TYC 2162-17-1) is a 8.6^m star discovered to be eclipsing variable by Hoffmeister [1935] with a period of about 2.2 days. Further photometric observations were summarised in Khaliullina and Khaliullin [1988] together with the estimation of parameters of the photometric orbit and its B0 V and B0.5 V stellar component assuming mass-luminosity relation. The fit of multicolor light curve contains third light of about 13% suggesting stellar companion of spectral class B4 V. Binary exhibits apsidal motion with a period of about 36 years as can be seen from times of minima in work Khaliullina [1987], where it is suggested that DR Vul might be quadruple system. Additional times of minima summarised in Wolf et al. [2019] led to the conclusion of only a triple system nicely described by LITE with the outer period of 66 years. Summary of know properties of the system can be found in tables 3.7 and 3.8. The distance to the system according to Khaliullina and Khaliullin [1988] from estimated absolute luminosities is about $1.2\,\mathrm{kpc}$ with corresponding parallax $\pi = 0.83\,\mathrm{mas}$, which is slightly less then Gaia Collaboration [2020] parallax $\pi = (0.74 \pm 0.03)\,\mathrm{mas}$ giving the distance $d = (1.34 \pm 0.06)\,\mathrm{kpc}$. It is important to mention quite a large absorption of light ($A_V \approx 1.8\,^{\mathrm{m}}$ due to dust in the galactic plane given the low galactic latitude $\lambda \approx -4°$ of the star. The star has an entry in Multiple Star Catalogue Tokovinin [2018a]. To the author's knowledge, the system was never investigated using spectroscopic methods.

In our analysis we have used 13 spectra taken between years 2003 and 2010 by M. Wolf (12), M. Tlamicha (6), L. Řezba (5), J. Fuchs (2), J. Čechura, P. Habuda, D. Huja, P. Chadima, L. Kotková, T. Krejčová, B. Kučerová, P. Pokorný, T. Rieb, P. Škoda, M. Šlechta, J. Sloup, P. Švaříček and P. Zasche (1). The mean signal-to-noise ratio of the spectra is about $S/N = 130$, the least robust set of spectra among the three objects. The main complication for disentanglement of spectra was apparent already at the first view - the spectra contain strong interstellar lines. As a reference during our work, we used the list of diffuse interstellar bands by Hobbs et al. [2008]. Most intense bands were eliminated and replaced by 1.0 flux before disentanglement. We needed to formally decompose into spectra of 5 components (3 stellar, telluric, and interstellar spectra). The orbit of the third body from LITE is known more precisely than we can hope to obtain from our data, so it was fixed during all our attempts. Because of poor quality, low number, and a lot of components, we were not able to directly solve for the orbit of central binary - `KOREL` was able to stop at radial velocity semiamplitudes in the range of $70\,\mathrm{km/s} - 350\,\mathrm{km/s}$. Therefore we computed expected semiamplitude from photometrical parameters and tables Harmanec [1988] as $K_1 = 230\,\mathrm{km/s}$ and $q = 0.937$ and just disentangle the spectra given fixed elements. This was done first for the spectrum of central binary and then for the spectrum of the third star in three spectral intervals (left of Hα profile where there is no contribution of central binary, on Hα, right of Hα where there is no contribution of telluric lines) for greater stability of the process. The resulting spectra of stellar components can be seen in figure 3.7.

Spectra of components A and B are quite similar, containing line Hα, line of neutral helium HeI at $\lambda = 6678\,\text{Å}$ and lines of ionized carbon CII at $\lambda = 6578\,\text{Å}\,\&\,6583\,\text{Å}$. The silicon lines are not present as well as lines of higher ion-

Table 3.7: Photometric orbital parameters of DR Vul according to Wolf et al. [2019]

T_0 (prim. ecl.)	$(2\,440\,300.7340 \pm 0.0005)\,\mathrm{d}$
P_s	$(2.250\,873\,14 \pm 0.000\,000\,05)\,\mathrm{d}$
e	0.0949 ± 0.0004
ω_0	$(269.9 \pm 0.6)°$
$\dot{\omega}$	$(9.96 \pm 0.10)\,°/\mathrm{y}$
i	$(88.3 \pm 0.3)°$
T_3	$(2\,454\,270 \pm 50)\,\mathrm{d}$
P_3	$(66.4 \pm 0.1)\,\mathrm{y}$
A_3	$(0.066 \pm 0.001)\,\mathrm{d}$
e_3	0.69 ± 0.01
ω_3	$(99.0 \pm 1.5)°$
$f(M_3)$	$0.348\,\mathrm{M_\odot}$
$K_{1,2}$	$7.11\,\mathrm{km/s}$

Table 3.8: Parameters of constituents of DR Vul system according to Khaliullina and Khaliullin [1988]

	primary	secondary	third light
V	$9.437^{\,\mathrm{m}}$	$9.699^{\,\mathrm{m}}$	$10.732^{\,\mathrm{m}}$
$B-V$	$0.247^{\,\mathrm{m}}$	$0.244^{\,\mathrm{m}}$	$0.321^{\,\mathrm{m}}$
A_V	$1.85^{\,\mathrm{m}}$	$1.75^{\,\mathrm{m}}$	$1.66^{\,\mathrm{m}}$
R/a	0.227 ± 0.003	0.206 ± 0.003	
R	$4.8\,\mathrm{R_\odot}$	$4.4\,\mathrm{R_\odot}$	$\approx 3.2\,\mathrm{R_\odot}$[†]
M	$13.2\,\mathrm{M_\odot}$	$12.1\,\mathrm{M_\odot}$	$\approx 5\,\mathrm{M_\odot}$[†]
T_{eff}	$29\,000\,\mathrm{K}$	$28\,000\,\mathrm{K}$	$\approx 17\,000\,\mathrm{K}$[†]
L	$1.47 \cdot 10^4\,\mathrm{L_\odot}$	$1.05 \cdot 10^4\,\mathrm{L_\odot}$	$\approx 800\,\mathrm{L_\odot}$[†]

[†] determined from spectral class B4 using Harmanec [1988]

Figure 3.7: Disentangled spectra of components of DR Vulpeculae
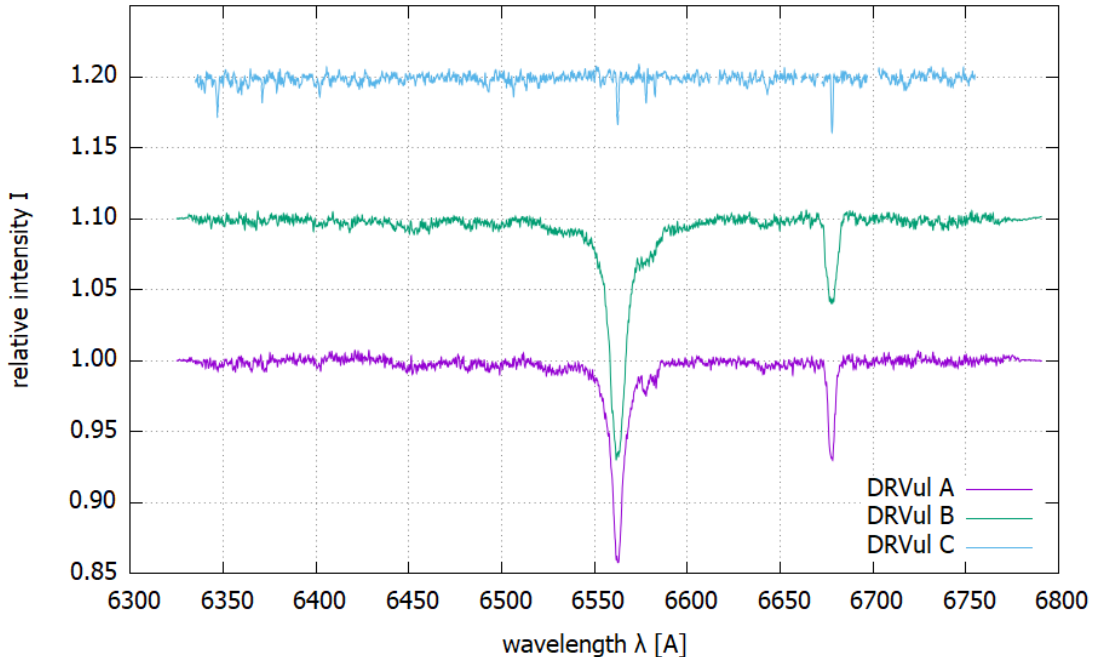
From bottom to top: spectrum of component A, spectrum of dimmer component B shifted by 0.1 upwards, spectrum of component C shifted by 0.2 upwards. Spectra of components are normalized to common continuum level.

ized species. Therefore, we can estimate the spectral class of the stars as B0-B1 in accordance with previous works. The spectrum of the third component contains additional lines of ionized silicon SiII at $\lambda = 6347\,\text{Å}\,\&\,6371\,\text{Å}$ that are less prominent than the helium line and possibly lines of neon NeI at $\lambda = 6402\,\text{Å}\,\&\,6506\,\text{Å}$. We estimate the spectral class of the third component as B3-B4 for which we get the mass $M_C = (5.5 \pm 1.0)\,\text{M}_\odot$ according to Harmanec [1988]. The lines of central binary are quite broad, with helium line full-width of about $7\,\text{Å}$ for component A and $10\,\text{Å}$ for component B. The third component C exhibits narrow lines of width about $2\,\text{Å}$ comparable to the width of telluric lines. We can crudely estimate rotational velocities of components to be $v_A \approx v_A \sin i \approx 320\,\text{km/s}$, $v_B \approx v_B \sin i \approx 450\,\text{km/s}$ and $v_C \sin i < 100\,\text{km/s}$ resulting in orbital periods of about $P_A \approx 18\,\text{h}$ and $P_B \approx 12\,\text{h}$ thus clearly rotating super-synchronously. We can not infer the limit on the rotational period of the third component because of the unknown orientation of its rotational axis.

To estimate the amplitude of radial velocities of the binary, we search the (K_1, q) space via KOREL three-star disentanglement using the part of spectra tightly around the helium line and recording the sum of spectral residuals. Other parameters were fixed using the photometric orbital solution. We note that for unrealistically small velocities ($< 100\,\text{km/s}$ the residuals were quite low, but the disentangled spectra had a warped continuum, and the lines themselves were not visible. For too large velocities, the residuals got large, and disentangled spectra of components A and B were flat while spectrum C contained an average of the input spectra. The diagram of residuals as a function of primary star semiamplitude K_1 and mass ratio q in realistic ranges can be seen in figure 3.8. As a next step, we allow KOREL to fit for K_1 and q around minima of

27

Table 3.9: Some parameters of DR Vul central binary - our work

a	$(20.1 \pm 0.6)\,\mathrm{R}_\odot$
R_1	$(4.56 \pm 0.15)\,\mathrm{R}_\odot$
R_2	$(4.14 \pm 0.14)\,\mathrm{R}_\odot$
M_1	$(11.4 \pm 1.1)\,\mathrm{M}_\odot$
M_2	$(10.1 \pm 1.0)\,\mathrm{M}_\odot$

the heatmap (K_1, q). We obtained $K_1 = (213 \pm 6)\,\mathrm{km/s}$ and $q = 0.884 \pm 0.045$ (resp. $K_2 = (241 \pm 11)\,\mathrm{km/s}$), where the errors were estimated from the $O - C$ of measured radial velocities. Using the equations in chapter 1.1 and some photometric quantities from Khaliullina and Khaliullin [1988], we can obtain physical parameters and semimajor axis of the orbit of central binary presented in table 3.9, that are slightly smaller than those in Khaliullina and Khaliullin [1988], and appropriate to B1 stars mainly due to a smaller semimajor axis. If we assume mass of third star to be about $M_3 = (5 \pm 1)\,\mathrm{M}_\odot$ we get the inclination of the outer orbit from the massfunction as $\sin i_3 = 1.2 \pm 0.3$ that is contrary to the theoretical prediction for $0.74 < i_3 < 0.79$ given the mutual inclination about $40°$. On the other hand, if we assume this inclination and observed massfunction, we arrive at the mass of the third star of about $M_3 \approx 8.5\,\mathrm{M}_\odot$ which is too massive for a star to produce the observed spectra and color indexes.

Figure 3.8: Map of residuals of helium line spectra of DR Vul on K_1, q
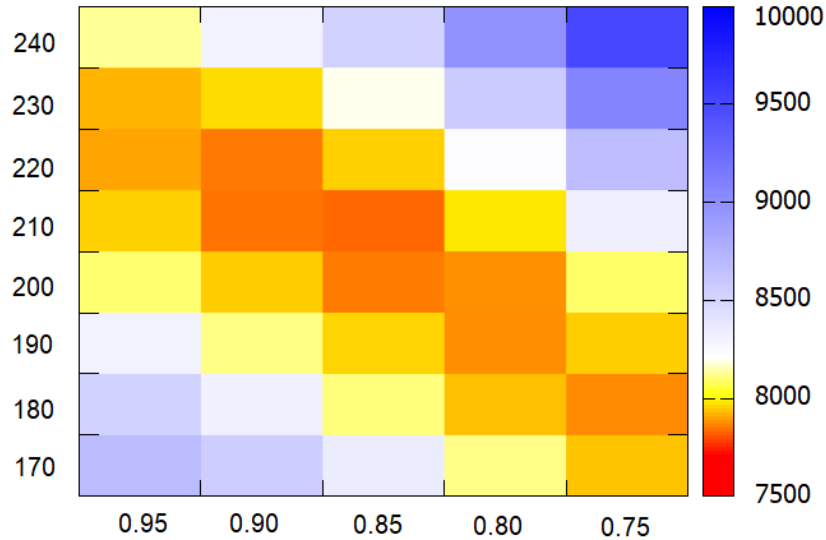
x-axis mass ratio q, y-axis primary star radial velocity semiamplitude K_1 in km/s.

3.4 Statistical considerations

We calculated several timescales according to equations in chapter 1.2 and equations 1.36, 1.37, 1.40, and compared them with main sequence lifespan of the more massive component given as approximately $\tau_{MS} \approx 10^{10}$ y $\cdot (M/M_\odot)^{-2.5}$ for our systems presented in table 3.10. For all systems, the circularisation timescale is about a tenth of the system's lifetime before the start of the mass transfer phase. V335 Ser components have slow rotation speeds in accordance with quite short synchronization times. The observed apsidal precession in work Lacy et al. [2012] is of the expected order of magnitude. In the case of BW Boo the age of the system was estimated to $\approx 1 \cdot 10^7$ y by Glazunova [2011]. We can see that the slow rotation of the components and eccentric orbit are conceivable even without the third body's presence. The detection of apsidal rotation should be possible, but as in the case of V335 Ser, we are not going to be able to cover the whole period. With precise enough photometric models, there is a possibility of detection of changes in the inclination of the primary orbit happening on the timescale similar to τ_{Kozai}. The system of DR Vul is the most interesting one - here, the stars rotate quicker than they should - we are expecting synchronous rotation given the short synchronization timescale. The observed apsidal period of about 3.6 y is conceivable given the crudeness of our estimated stellar parameters. The Kozai period is too long for any practical determination.

Table 3.10: Approximate calculated timescales of the observed systems in years

| system	τ_{MS}	τ_{circ}	$\tau_{synchr,1}$	$\tau_{synchr,2}$	U	τ_{Kozai}
V335 Ser	$1.5 \cdot 10^9$	$1.2 \cdot 10^8$	$5 \cdot 10^4$	$9 \cdot 10^4$	550	–
BW Boo	$2 \cdot 10^9$	$2.2 \cdot 10^8$	$9 \cdot 10^4$	$1.2 \cdot 10^3$	800	$5 \cdot 10^3$
DR Vul	$2 \cdot 10^7$	$2.0 \cdot 10^6$	$2 \cdot 10^3$	$3 \cdot 10^3$	≈ 10	$3 \cdot 10^5$

Finally, we look at the position of our systems among the population of double and multiple star systems. For this application, we are using the binary star catalogue Pourbaix et al. [2004] of spectroscopic orbits and the Multiple star catalogue by Tokovinin [2018b] containing systems with three or more components. In diagrams of the period versus eccentricity at figure 3.9 we see that our systems are common members of short period eccentric system distribution. We note that more than half of eccentric binary systems at these periods have already discovered companions. Ratio of inner and outer periods for DR Vul is about $P_3/P_1 = 10\,700$ at $e = 0.69$, for BW Boo we approximate $P_3/P_1 \approx 1000$ therefore comfortably fulfilling the criterion of stability 1.35. In the case of BW Boo we obtain a limiting eccentricity of about 0.85. We can see the position of our systems among the systems with determined orbits from Tokovinin [2018b] in period-period and eccentricity of outer orbit vs. period ratio at the figure 3.10. Again our systems lie inside the space of the general population. We note that the criterion 1.35 is not fulfilled well by the systems, with some systems lying outside of the bound.

Figure 3.9: The distribution of system periods P and eccentricities e.
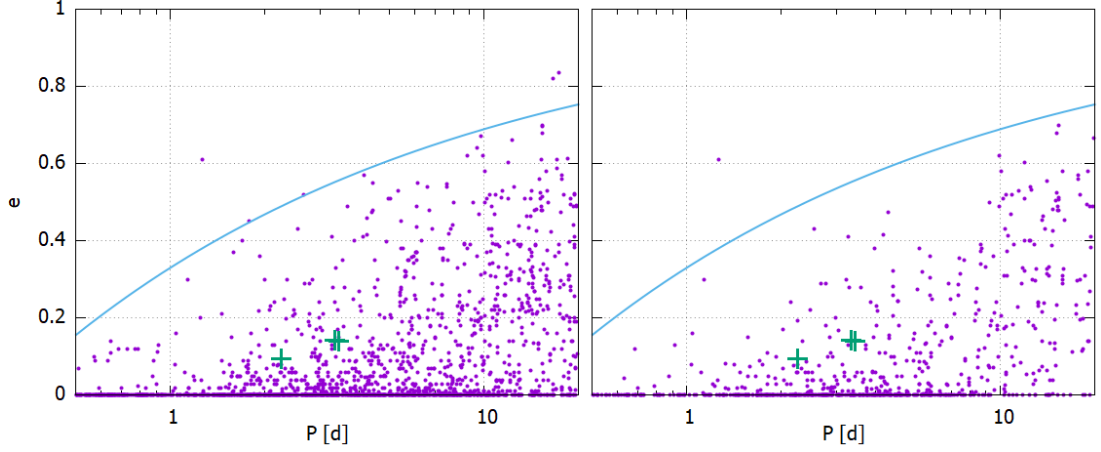
Left: double star catalogue of Pourbaix et al. [2004], right: multiple star catalogue
of Tokovinin [2018b]. Orbits from catalogues are presented in purple dots; our systems are
represented by green crosses from left to right DR Vul, BW Boo, V335 Ser. The blue line
denotes the envelope of observed orbits by Pourbaix et al. [2004] given by a constant value of
$$P(1-e)^3.$$

Figure 3.10: The distribution of system periods P_1, P_3 and outer eccentricities e_3.
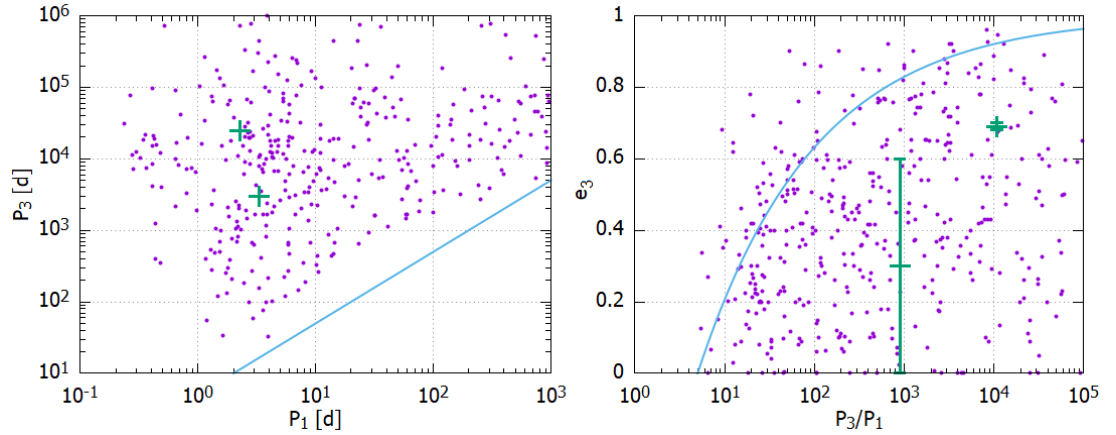
Left: distribution of outer period P_3 against inner period P_1, right: distribution
of eccentricities of outer orbit e_3 against period ratio P_3/P_1. Systems from catalogue
of Tokovinin [2018b] are denoted by purple dots, our systems are represented by green crosses:
left: DR Vul top, BW Boo bottom, right: BW Boo left, DR Vul right.
The blue line denotes the stability criterion 1.35.

Conclusion

We obtained spectra of components of the V335 Serpentis presenting narrow lines of a slowly rotating early A stars and measured 33 new radial velocities agreeing with the orbital solution by Lacy et al. [2012]. We were not able to detect a possible third companion in the spectral residuals. Assuming it to be a main sequence star, we estimated it's of no earlier type than mid-K dwarf if present. The star is going to be covered by TESS mission in the summer of 2022.

Spectral disentanglement of system BW Boo yielded an early A class spectrum of primary, mid G class spectrum of secondary, and even a late G class spectrum of the third component together with a set of 21 radial velocities. We modeled the TESS lightcurve of the system in two cases of third light ($l_3 = 0$ and $l_3 = 0.15$ expected from the spectral class of the third component), arriving to two sets of physical parameters of the central binary components and their mutual orbit. We are not able to distinguish between these two models from TESS single-color photometry alone. The third component seems to be on orbit with the binary with a period of about $3000\,\mathrm{d}$ and radial velocity semiamplitudes of about $5\,\mathrm{km/s}$. We note that to determine the orbit of this body, a study on eclipse timing variation of the binary is needed. Expected amplitude of the changes is about $\Delta t \approx 3 \cdot 10^{-3}\,\mathrm{d} \approx 5\,\mathrm{min}$ which is achievable using CCD detectors even on sub $0.5\,\mathrm{m}$ telescopes. The star is therefore a suitable target for amateur and public observatories.

Analysis of the system DR Vul was complicated by the presence of diffuse interstellar bands in the spectra and rapid apsidal precession. We were able to obtain the spectra of all three known components confirming their stellar classification as B0-1, B0-1, and B3-4. From the 13 spectra, we estimated the radial velocity amplitudes of the central components to be $(213 \pm 6)\,\mathrm{km/s}$ and $(241 \pm 11)\,\mathrm{km/s}$ and computed physical parameters and orbit of the binary using the photometric parameters by Wolf et al. [2019]. We noted that the rotational velocity of the stars determined from helium and carbon lines broadening is super-synchronous contrary to the synchronization timescale of the system of about a thousand years. We estimated the relative inclination of the orbit $\sin i = 1.2 \pm 0.3$ to be quite far from the $i \approx 40°$ driven by Kozai cycles with tidal friction. The orbits may be complanar instead. To better estimate the orbits, there is a need to obtain spectra in ranges of wavelengths where there are fewer other lines (atmosphere, interstellar medium) present - for example, in the blue region of Hβ and Hγ lines. The star is going to be covered by TESS mission in the summer of 2022.

All obtained spectra of the components can be used in atmosphere modeling to independently estimate some of the stellar parameters.

Bibliography

U. Bastian and E. Born. The variability type and period of HD 143213. *Information Bulletin on Variable Stars*, 4536:1, December 1997.

U. Bastian and E. Born. Precise lightcurve elements for HD 143213. *Information Bulletin on Variable Stars*, 4590:1, April 1998.

T. Borkovits, B. Érdi, E. Forgács-Dajka, and T. Kovács. On the detectability of long period perturbations in close hierarchical triple stellar systems. *A&A*, 398:1091–1102, February 2003. doi: 10.1051/0004-6361:20021688.

T. Borkovits, Sz. Csizmadia, E. Forgács-Dajka, and T. Hegedüs. Transit timing variations in eccentric hierarchical triple exoplanetary systems. I. Perturbations on the time scale of the orbital period of the perturber. *A&A*, 528:A53, April 2011. doi: 10.1051/0004-6361/201015867.

Z. Bozkurt. The first spectroscopic and photometric solutions of the eclipsing binary, V335 Ser. *New A*, 16(6):412–419, October 2011. doi: 10.1016/j.newast.2011.03.007.

Daniel Fabrycky and Scott Tremaine. Shrinking Binary and Planetary Orbits by Kozai Cycles with Tidal Friction. *ApJ*, 669(2):1298–1315, November 2007. doi: 10.1086/521702.

Gaia Collaboration. VizieR Online Data Catalog: Gaia EDR3 (Gaia Collaboration, 2020). *VizieR Online Data Catalog*, art. I/350, November 2020.

A. Gimenez. General-relativistic periastron advances in eclipsing binary systems. *ApJ*, 297:405–412, October 1985. doi: 10.1086/163539.

A. Giménez and J. M. García-Pelayo. A New Method for the Analysis of Apsidal Motions in Eclipsing Binaries. *Ap&SS*, 92(1):203–222, May 1983. doi: 10.1007/BF00653602.

L. V. Glazunova. Absolute parameters of the close binary BW Boo with a superasynchronous A2m primary component. *Astronomy Letters*, 37(6):414–419, June 2011. doi: 10.1134/S1063773711050033.

W. Gorza and J. F. Heard. Radial Velocity Observations of the Eclipsing System HD 128661. *Information Bulletin on Variable Stars*, 396:1, October 1969.

P. Hadrava. KOREL - User's guide. *Publications of the Astronomical Institute of the Czechoslovak Academy of Sciences*, 92:15–35, January 2004.

P. Harmanec, J. Lipták, P. Koubský, H. Božić, J. Labadie-Bartz, M. Šlechta, S. Yang, and A. Harmanec. A new study of the spectroscopic binary 7 Vul with a Be star primary. *A&A*, 639:A32, July 2020. doi: 10.1051/0004-6361/202037964.

Petr Harmanec. Stellar Masses and Radii Based on Modern Binary Data. *Bulletin of the Astronomical Institutes of Czechoslovakia*, 39:329, December 1988.

L. M. Hobbs, D. G. York, T. P. Snow, T. Oka, J. A. Thorburn, M. Bishof, S. D. Friedman, B. J. McCall, B. Rachford, P. Sonnentrucker, and D. E. Welty. A Catalog of Diffuse Interstellar Bands in the Spectrum of HD 204827. *ApJ*, 680 (2):1256–1270, June 2008. doi: 10.1086/587930.

Cuno Hoffmeister. 162 neue Veräderliche. *Astronomische Nachrichten*, 255:401, June 1935. doi: 10.1002/asna.19352552202.

G. Jackisch. HD 128661, Probably an Eclipsing Variable. *Information Bulletin on Variable Stars*, 314:1, November 1968.

Jon M. Jenkins, Joseph D. Twicken, Sean McCauliff, Jennifer Campbell, Dwight Sanderfer, David Lung, Masoud Mansouri-Samani, Forrest Girouard, Peter Tenenbaum, Todd Klaus, Jeffrey C. Smith, Douglas A. Caldwell, A. D. Chacon, Christopher Henze, Cory Heiges, David W. Latham, Edward Morgan, Daryl Swade, Stephen Rinehart, and Roland Vanderspek. The TESS science processing operations center. In Gianluca Chiozzi and Juan C. Guzman, editors, *Software and Cyberinfrastructure for Astronomy IV*, volume 9913 of *Society of Photo-Optical Instrumentation Engineers (SPIE) Conference Series*, page 99133E, August 2016. doi: 10.1117/12.2233418.

A. I. Khaliullina. DR Vulpeculae : the quadruple system. *MNRAS*, 225:425–436, March 1987. doi: 10.1093/mnras/225.2.425.

A. I. Khaliullina and Kh. F. Khaliullin. Photometric investigation of the eclipsing binary star DR Vul. Orbital parameters and apsidal motion. *AZh*, 65:108–116, February 1988.

L. G. Kiseleva, P. P. Eggleton, and S. Mikkola. Tidal friction in triple stars. *MNRAS*, 300(1):292–302, October 1998. doi: 10.1046/j.1365-8711.1998.01903. x.

Maria Kurpinska. BW Bootis - an Algol Type Eclipsing Variable. *Information Bulletin on Variable Stars*, 1007:1, June 1975.

Claud H. Sandberg Lacy, Francis C. Fekel, and Antonio Claret. ABSOLUTE PROPERTIES OF THE ECLIPSING BINARY STAR v335 SERPENTIS. *The Astronomical Journal*, 144(2):63, jul 2012. doi: 10.1088/0004-6256/144/2/63. URL https://doi.org/10.1088/0004-6256/144/2/63.

Valeri Makarov, Ulrich Bastian, Erik Hoeg, Volkmar Grossmann, and Andreas Wicenec. 35 new bright medium- and high-amplitude variables discovered by the TYCHO instrument of the HIPPARCOS satellite. *Information Bulletin on Variable Stars*, 4118:1, November 1994.

A. J. Pickles. A Stellar Spectral Flux Library: 1150-25000 Å. *PASP*, 110(749): 863–878, July 1998. doi: 10.1086/316197.

D. Pourbaix, A. A. Tokovinin, A. H. Batten, F. C. Fekel, W. I. Hartkopf, H. Levato, N. I. Morrell, G. Torres, and S. Udry. S_B^9: The ninth catalogue of spectroscopic binary orbits. *A&A*, 424:727–732, September 2004. doi: 10.1051/0004-6361:20041213.

Andrej Prša. *Modeling and Analysis of Eclipsing Binary Stars; The theory and design principles of PHOEBE.* 2018. doi: 10.1088/978-0-7503-1287-5.

Andrej Prša and Petr Harmanec. *PHOEBE manual.* 2010. avaible at `http://phoebe-project.org/static/legacy/docs/phoebe_manual.pdf`.

S. Soderhjelm. The three-body problem and eclipsing binaries. Application to Algol and lambda Tauri. *A&A*, 42:229–236, August 1975.

T. E. Sterne. Apsidal motion in binary stars. *MNRAS*, 99:451–462, March 1939. doi: 10.1093/mnras/99.5.451.

Jean-Louis Tassoul. On Synchronization in Early-Type Binaries. *ApJ*, 322:856, November 1987. doi: 10.1086/165780.

Jean-Louis Tassoul. On Orbital Circularization in Detached Close Binaries. *ApJ*, 324:L71, January 1988. doi: 10.1086/185094.

A. Tokovinin. Dynamics of Multiple Stars: Observations. In Nicole St. -Louis and Anthony F. J. Moffat, editors, *Massive Stars in Interactive Binaries*, volume 367 of *Astronomical Society of the Pacific Conference Series*, page 615, January 2007.

A. Tokovinin. VizieR Online Data Catalog: Updated Multiple Star Catalog (MSC): Sept 2021 (Tokovinin, 2018). *VizieR Online Data Catalog*, art. J/ApJS/235/6, August 2018a.

A. Tokovinin, S. Thomas, M. Sterzik, and S. Udry. Tertiary companions to close spectroscopic binaries. *A&A*, 450(2):681–693, May 2006. doi: 10.1051/0004-6361:20054427.

Andrei Tokovinin. The Updated Multiple Star Catalog. *ApJS*, 235(1):6, March 2018b. doi: 10.3847/1538-4365/aaa1a5.

Roland Vanderspek, John P. Doty, Michael Fausnaugh, Jesus Noel S. Villaseñor, Jon M. Jenkis, Zachory K. Berta-Thompson, Christopher J. Burke, and George R. Ricker. *TESS Instrument Handbook.* December 2018. available online at `https://archive.stsci.edu/files/live/sites/mast/files/home/missions-and-data/active-missions/tess/_documents/TESS_Instrument_Handbook_v0.1.pdf`.

P. Škoda and P. Hadrava. Fourier Disentangling Using the Technology of Virtual Observatory. In A. Prša and M. Zejda, editors, *Binaries - Key to Comprehension of the Universe*, volume 435 of *Astronomical Society of the Pacific Conference Series*, page 71, December 2010.

Petr Škoda, Petr Hadrava, and Jan Fuchs. VO-KOREL: A Fourier Disentangling Service of the Virtual Observatory. In Mercedes T. Richards and Ivan Hubeny, editors, *From Interacting Binaries to Exoplanets: Essential Modeling Tools*, volume 282, pages 403–404, April 2012. doi: 10.1017/S1743921311027931.

M. Wolf, P. Zasche, H. Kučáková, M. Mašek, K. Hoňková, J. Juryšek, A. Paschke, L. Šmelcer, and M. Zejda. Triple Eccentric Systems V0345 Lac, YY Sgr, and DR Vul. *Acta Astron.*, 69(1):63–78, March 2019. doi: 10.32023/0001-5237/69.1.5.

P. Zasche. PHOEBE - step by step manual. *Open European Journal on Variable Stars*, 176:10, March 2016.

List of Figures

List of Tables

A. Measured radial velocities of the systems using `KOREL`

The following tables contain results of radial velocity measurement using `KOREL`. We note that `KOREL` measures relative motions, it is unable to provide systematic γ velocities by design. We present directly computed velocities, it is to note that residuals of telluric lines radial velocities can be used to estimate error of the measurement or used as a fine calibration correction by substracting them from the measured radial velocities of the stellar components. In case of BW Bootis the velocity of the third component can have nonzero constant shift relative to the central binary.

Table A.1: Measured radial velocities of components of BW Boo

$HJD - 2\,400\,000$	RV_A	RV_B	RV_C	RV_{tell} O-C
[d]	[km/s]	[km/s]	[km/s]	[km/s]
54217,443	-12,83	26,91	0,74	0,28
54218,391	-64,02	115,81	-3,21	-0,24
54219,367	48,16	-88,32	-2,48	-2,24
54239,363	50,54	-84,23	-2,09	0,41
54266,357	64,06	-112,46	-1,12	-0,07
54924,382	-67,87	120,08	-1,39	-0,10
55274,429	-79,37	138,58	0,94	-0,54
55295,405	1,24	-3,62	-0,72	-1,05
55316,450	60,89	-112,15	0,47	0,43
55622,520	49,72	-87,92	1,33	2,79
56357,588	-81,27	134,94	4,54	-0,46
56393,444	27,29	-53,72	2,87	-0,21
56407,410	-63,08	104,94	3,00	-0,23
57079,482	64,30	-108,78	-0,67	0,37
57117,474	-75,86	137,56	-0,54	1,48
57126,432	51,27	-89,51	0,21	0,32
57147,401	-70,06	126,83	0,33	0,20
57160,529	-43,51	82,19	-1,44	0,61
57294,266	-82,22	147,94	3,10	0,14
57868,364	8,69	-13,11	0,42	1,10
57876,352	49,14	-85,49	2,07	1,14
O-C rms	1,92	1,66	1,98	1,00

Table A.2: Radial velocities of V335 Ser in the reference frame of the binary

HJD $-$ 2 400 000	RV_A	RV_B	RV_{tell} O-C
[d]	[km/s]	[km/s]	[km/s]
53454.512	-78.67	90.92	0.80
53524.475	-58.38	65.78	0.54
53846.516	105.84	-117.00	1.53
53860.504	110.66	-126.25	-1.16
53898.463	113.46	-124.29	1.02
54203.500	-100.85	111.89	-0.23
54210.484	-98.19	113.49	0.57
54217.489	-93.50	107.90	1.94
54275.417	-51.55	57.90	-0.46
54300.362	-89.81	100.49	-0.03
54314.362	-74.10	83.63	-0.32
54603.395	-88.23	98.54	0.61
54616.362	81.96	-93.68	-1.00
54650.366	106.02	-120.55	-0.42
54924.495	-100.78	111.73	-0.25
54933.587	105.77	-117.16	0.58
54937.476	25.92	-28.94	0.62
55295.484	104.59	-120.35	-0.74
55316.474	108.26	-123.12	-0.72
55385.404	111.01	-124.24	-0.35
55386.410	-73.81	83.09	0.07
55391.368	13.87	-10.69	0.13
55392.342	110.11	-124.84	-0.42
55398.414	33.83	-39.38	-0.09
55602.622	110.17	-126.10	0.02
55616.601	108.06	-125.59	-1.30
55642.532	-78.74	84.61	-0.56
55661.557	100.91	-112.74	0.70
55671.475	101.61	-115.63	-0.20
56043.426	17.90	-21.53	-0.26
56407.462	-57.65	62.32	-1.17
56527.294	112.74	-126.29	0.16
O-C rms	1.17	1.40	0.80